Activated rice husk biochar for azo dye removal: Batch adsorption, kinetics and thermodynamic studies

Arivumani V.[1]*, Singh V.[2], Geetha C.[3] and Senthilkumar C.[4]

[1]Department of Architecture, Sigma College of Architecture, Anducode, Tamil Nadu-629168, India

[2]Department of Civil Engineering, Integral University, Lucknow, Uttar Pradesh-226026, India

[3]Department of Chemistry, Rajalakshmi Engineering College (Autonomous), Chennai, Tamil Nadu-602105, India
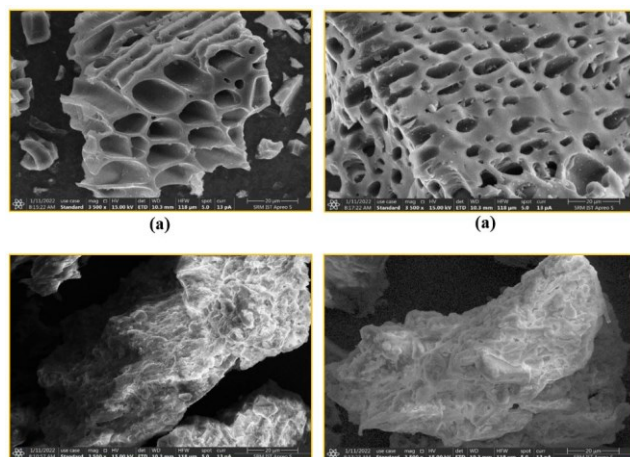
[4]Department of Mechanical Engineering, SNS College of Technology, Tamil Nadu-641035, India

Graphical abstract

Abstract

The study aimed to analyze the adsorption behaviour of an activated rice husk biochar adsorbent in batch mode to expunge azo dye concentrations depletion from liquid solvents. The biochar adsorbent was formulated using different chemical synthesis processes, and its surface region was assessed using Nitrogen retention. The existence of the particular azo dyes was verified through SEM and EDX examinations. Additionally, XRD analysis was conducted to examine the intensity and crystalline structure of the activated biochar adsorbent. A batch mode study was conducted to ascertain the ideal adsorption parameters, including pH, contact time, biochar dose, and azo dye concentration. The adsorption kinetic studies supported the notion of a favourable adsorption interaction occurring through the mutual influence of the adsorbed matter and the adsorbing substrate. Most isotherm studies were well-fitted with regression values of isotherm models, indicating an adsorption process with non-uniform monolayer formation. Thermodynamic investigations validated that the binding forces between the adsorptive and the adsorbing phase are endothermic, and a significant amount of spent adsorbent was successfully recovered using a strong hydrochloric acid desorption process.

Keywords: Biosorption, rice husk ash, azo dyes, batch studies, kinetic modelling, desorption

1. Introduction

Water pollution has been a long-standing and severe issue, primarily driven by the rapid release of chemicals and toxic minerals from industrial activities. These alterations in water's physical and chemical properties can pose significant health and environmental risks due to their inherent toxicity. Access to clean water is essential for the survival of all living organisms. However, the quality of water has been deteriorating due to the presence of toxic pollutants and various organic and inorganic pathogens. What makes these pollutants particularly concerning is that they are often non-degradable and can have harmful effects even at deficient concentrations (Priya *et al.* 2022). This underscores the critical importance of addressing water pollution and ensuring the availability of safe and clean water sources. Water pollution is a grave concern, exacerbated by the introduction of various harmful substances into natural water sources through industrial activities and human actions. These contaminants encompass heavy metals, dyes, microbes, fertilizers, pesticides, and other compounds (Regti1 *et al.* 2017). Notably, chemical dyes are a significant contributor to water toxicity. It's important to recognize that while dyes serve essential purposes across diverse industries, their improper disposal and release into the environment can harm aquatic ecosystems and human well-being. Thus, a pressing challenge is balancing the indispensable use of dyes for various applications and the imperative to mitigate their adverse environmental effects.

The global issue of excessive industrial wastewater discharge into natural water bodies poses a significant challenge. This wastewater often contains non-degradable pollutants, including heavy metals and dyes, which can lead to the generation of harmful byproducts. Particularly concerning is the presence of dye pollution in the

effluents from textile industries, as it can result in water toxicity and transform natural water sources into hazardous environments (Bouras *et al.* 2015). This underscores the urgent need for effective strategies to manage and treat industrial wastewater, minimizing its detrimental impact on aquatic ecosystems and public health. Eliminating dye pollution from water solutions is a challenging task that often requires substantial capital investment. Various treatment methods address this issue, including membrane separation, adsorption, chemical precipitation, coagulation and flocculation, and ion exchange. These techniques have been widely utilized for effectively eliminating dye contaminants from water sources, as highlighted in a study by Xi and colleagues in 2020.

The conventional methods mentioned have limitations such as secondary sludge generation, potentially harmful chemicals, the need for skilled personnel, and high investment costs. Consequently, there is a growing demand for innovative treatment approaches that are cost-effective and environmentally friendly. Among these methods, the adsorption process has recently gained significant attention as an efficient means of removing pollutants from aqueous solutions. This approach boasts minimal investment requirements and does not result in the formation of secondary sludge during wastewater treatment. The adsorption process has proven highly efficient when employing suitable adsorbent materials (Labied *et al.* 2018). In this process, pollutants are captured and accumulate at the external aspect of the adsorbing medium owing to attractive forces such as van der Waals. A wide range of organic and inorganic materials have been employed as adsorbents to capture pollutants from wastewater (Venkatraman *et al.* 2021). Different types of dyes, such as Acid Brown, Reactive Red, and Methylene Blue, exist depending on the industrial processes, and the choice of adsorbent material can significantly influence the efficiency of selective dye removal. The selection nature of the adsorbing agent plays a pivotal role in achieving efficient removal rates during the adsorption process. In this investigation, activated biochar, derived explicitly from rice husks, was employed as the adsorbent material for removing Acid Brown and Methylene Blue azo dyes from synthetic solutions. These dyes, prevalent in effluents from various textile industries, can potentially induce aquatic toxicity and detrimental impacts on the nearby environment.

In this systematic testing, Rice Husk Biochar was used as the adsorbing medium designed to eliminate azo dyes by using batch adsorption to extract from fabricated solutions. Cultivating rice plants, which produce rice husks, consumes substantial groundwater for irrigation. This practice can result in the penetration of rice husk biochar into the soil, reaching depths of up to 6 meters. Consequently, the groundwater table has significantly diminished in various regions of Tamil Nadu, mainly due to the widespread availability and utilization of activated rice husk biochar. Therefore, the decision was made to employ this material to eradicate Acid Brown, Reactive Red, and Methylene Blue dyes from synthetic solutions. In this study, biochar derived from rice husks was utilized, and the effectiveness of azo dye removal was examined under various operational parameters in a batch adsorption process.

2. Materials and methodology

2.1. Biochar and stock solution preparation

Initially, Rice Husk Biochar was sourced from various forest areas, cleansed with water, and left to air-dry for 24 hours. Subsequently, it was cut into small fragments and subjected to continuous grinding. Following that, the sample underwent a 36-hour drying process at 200°C. After this heating procedure, the sample was blended with concentrated sulfuric acid to activate the adsorbent chemically, increasing its surface area. The activated charcoal sample was meticulously rinsed with double-distilled water and then placed in an oven at 80°C for 12 hours. To further boost the surface area of the prepared charcoal adsorbent, it underwent treatment with a hydrogen peroxide (H_2O_2) solution. The charcoal powder was immersed in the H_2O_2 solution for 24 hours and subjected to additional heating. After this treatment, the sample was collected, washed several times with distilled water, and made ready for further experimental usage. The transformation from biochar to biochar was achieved through additional heating and drying processes. Acid Brown and Methylene Blue, readily available in the local market and of analytical grade, were used to formulate synthetic solutions containing azo dyes. These dyes did not require further purification. Double-distilled water was added to these dyes, resulting in synthetic solutions with a total capacity of 1000 ml, which were used for all subsequent experimental procedures.

2.2. Characterization of biochar adsorbent

Using a surface area analyser, the adsorbent's specific surface area and pore structure were assessed through nitrogen adsorption at −196°C. To prepare the sample for analysis, it was held at 300°C for 3 hours to eliminate any residual gas or vacuum. The surface area (S_{BET}) of the Activated Rice Husk Biochar charcoal powder was determined utilizing the Brunauer–Emmett–Teller (BET) analysis method. The surface area analyzer helped derive both micropore (Su) and mesopore (Sm) areas through the Dubinin–Radushkevich (D–R) method, with the relationship $Sm = S_{BET} − Su$. By measuring the total volume of the pore (V_T) under relatively high pressure (P/Po~0.99) with liquid nitrogen, the total pore volume (V_T) was calculated. The micropore and mesopore volumes (V_u & V_m) were then determined using the $Vm = VT − Vu$ equation. The Barrett–Joyner–Halenda (BJH) model was employed to assess the pore size distribution, with the mean pore diameter (DP) being calculated using the formula $D_P = 4V_T/S_{BET}$.

Fourier Transform Infrared Spectroscopy (FTIR) was analysed to identify the functional groups and chemical characteristics of the prepared Activated Rice Husk Biochar charcoal powder. The analysis involved mixing 25 ml/L concentrated synthetic solutions containing the

targeted azo dyes employing 1 gram of the sorption agent. The solution displayed a pH reading of 6.0, and the blend was stirred in a rotary shaker at 200 rpm for 3 hours. The resulting suspension was employed for subsequent experiments. Investigations. FTIR analysis encompassed a scanning range of $400 - 4000$ cm^{-1} with a resolution of 4 cm^{-1}, and spectra were generated through 20 scans. Scanning Electron Microscopic (SEM) analysis, coupled with Energy Dispersive X-ray (EDX) analysis, was conducted with an operational spacing of 20 microns with a voltage of 15 kilovolts to verify the existence of the specified azo dyes affixed to the exterior of the adsorbent. This analysis also provided insights into the elemental and physical properties of the adsorbent. X-ray Diffraction (XRD) analysis was carried out to examine the crystalline structure of the activated rice husk powder, with data collected at different peaks using $CuK - \alpha -$ radiation at 40 kV and 250 mA.

2.3. Batch studies of adsorption

The batch process utilizing Activated Rice Husk Biochar activated carbon involved adjustments to several operational parameters at different intervals. These parameters included variations in pH levels, contact duration between azo dyes and the biochar adsorbent, changes in biochar dosage, adjustments to azo dye concentrations, and alterations in solution temperature. These experiments were conducted to assess how these factors influenced the efficiency of the adsorption process using Activated Rice Husk Biochar activated carbon. The pH of the synthetic solution containing azo dyes was adjusted within the range of 2.0 to 12.0 using buffer tablets, and the temperature was kept constant at 30°C with an equilibrium time of 1 hour. During the introductory stage of the batch adsorption research, the concentration of dyes containing azo groups was maintained at 50 mg/L in a 100 mL aqueous solution. To determine the optimal dosage of Activated Rice Husk biochar carbon, the quantity of adsorbent was varied from 0.5 to 3 g/L and mixed with the known concentrations of azo dyes and the contact time between the Activated Rice Husk Biochar adsorbent and the azo dye solution ranged from 10 to 120 minutes. The solution was introduced into a shaker and continuously agitated for 1 hour to achieve equilibrium. Equation 1 was employed to compute the quantity of azo dye adsorbed by the Activated Rice Husk Biochar adsorbent throughout this equilibrium phase.

$$q_t = \frac{(C_o - C_t)\ V}{m}\ ml/g \tag{1}$$

The Activated Rice Husk Biochar adsorbent and its uptake of azo dyes were denoted by q_t. In contrast, the azo dye solution's saturation level in the batch adsorption study was denoted by C_t. V represented the extent of the azo dye solution, and "m" indicates the system's gravitational pull. After the 1-hour equilibrium period, the solution was centrifuged for 5 minutes. The final suspension was then collected, and the concentration of azo dyes was determined using AAS (AA6300). Each analysis was performed in duplicate to obtain consistent values.

Equation 2 represents the mass balance approach of the adsorption system.

$$\% \text{ Removal} = \left[\frac{C_o - C_e}{C_o}\right] X100 \tag{2}$$

The starting and eventual concentrations of azo dyes in synthetic solutions as the process unfolds the equilibrium time was represented by C_o and C_e, respectively, in mg/L.

2.4. Adsorption isotherm studies

Isotherm studies are represented by an equation used to assess the transfer of adsorbate azo dye molecules from moving matter from the liquid medium to the adsorbent medium in a state of balance (Tovar *et al.* 2021). The isotherm studies described the interaction between adsorbate molecules and adsorption sites. This study employed different types of isotherm studies to examine how activated rice husk powder interacts with the selected azo dyes during adsorption.

2.4.1. Langmuir isotherm study

This study aimed to describe the point of equilibrium where the adsorption material and the gas phase interact. It sought to establish the relationship between solid and fluid concentrations in the isotherm, providing insights into the changes occurring during adsorption. The isotherm study follows a monolayer adsorption process on the surface of the adsorbent at specific relative pressures, reflecting its heterogeneous nature (Kumar *et al.* 2019). It assumes that the adsorbent and adsorbate binding mechanisms occur through chemical reactions. Equation 3 can be expressed as the Langmuir isotherm linear equation.

$$\frac{C_e}{q_e} = \frac{1}{K.q_{max}} + \frac{C_e}{q_{max}} \tag{3}$$

In this context, the symbols have the following meanings: C_e stands for the equilibrium concentration of the solution in ml/L, q_e represents the quantity of azo dyes adsorbed per gram (K), and q_{max} pertains to the constants found in the Langmuir isotherm equation, signifying the Adsorption efficiency and bonding intensity.

2.4.2. Freundlich isotherm study

The Freundlich isotherm study entails investigating changes in the quantity of adsorbed gas per unit mass of adsorbent while altering system pressure at a specific temperature, as outlined by Nathan *et al.* 2021. This isotherm model allows for multiple adsorption layers on the adsorbent surface and was developed based on heterogeneous surface adsorption. The linearized form of the isotherm model's equation can be represented as indicated in Equation 4.

$$\ln q_e = \ln k_f + \frac{1}{n}\ln C_e \tag{4}$$

In this context, the variables are defined as follows: q_e represents the held concentration of the adsorbate per gram, "n" signifies the adsorption potential, K_f is associated with adsorption volume and connected to the Freundlich constant, while C_e represents the Concentration in the adsorption steady state.

2.4.3. Sips isotherm study

The Sips isotherm model, which blends elements of both Langmuir and Freundlich isotherms, is utilized to forecast the behaviour of heterogeneous sites under restricted conditions, with the concentration of the adsorbate being disregarded (Mwandira *et al.* 2020). Commonly, this model characterizes a monolayer adsorption process. Equation 5 can express the linear form of the Sips model isotherm.

$$\frac{1}{q_e} = \frac{1}{Q_{max}K_s}\left(\frac{1}{C_e}\right)^{\frac{1}{n}} + \frac{1}{Q_{max}} \tag{5}$$

In this context, Q_{max} and K_s represent the adsorption capacity and equilibrium constant, respectively. Values are derived from the incline and intercept observed in linear graphical representations. The parameter 'n' indicates the degree of heterogeneity and falls within the range of 0 to 1.

2.4.4. Redlich-peterson (R-P) isotherm study

The R-P isotherm, also known as the three-factor empirical isotherm model, is derived from the amalgamation of Langmuir and Freundlich isotherm studies. This model is predicated on the distinctive adsorption mechanism between the adsorbate and adsorbent, and it doesn't conform to the monolayer process, as per its fundamental assumption (Khan *et al.* 2022). The linear representation of the R-P isotherm model can be described by Equation 6.

$$\ln(K_R\frac{C_e}{q_e} - 1) = b_R\ln C_e + \ln a_R \tag{6}$$

In this context, K_R represents the adsorption capacity constant derived from the linear plots of the R-P isotherm. Additionally, 'a_R' stands for the R-P isotherm constant, and 'b_R' signifies the exponent value, typically within the range of 0 to 1.

2.4.5. Fritz-schlunder isotherm study

This isotherm, sometimes referred to as experimental data across a broad range, is examined using a model with four parameters. It enhances analyzing adsorption behaviour using empirical relationships (Panda *et al.* 2020). The model's attributes can be resolved using non-linear regression analysis. The linear form of the Fritz-Schlunder isotherm model can be represented by Equation 7

$$q_e = \frac{q_{mFS}K_{FS}C_e}{1 + q_m C_e^{MFS}} \tag{7}$$

- In this context, the variables are defined as follows:
- q_{mFS} represents the maximum adsorption capacity in mg/g.
- K_{FS} stands for the constant in equilibrium time in mg/g.
- MFS denotes the model exponent.

2.4.6. Toth isotherm study

The Toth isotherm model was created to reduce the discrepancies that might occur when combined with experimental and equilibrium data from the Langmuir isotherm model. The Toth isotherm study elucidates the adsorption process across a wide range of azo dye concentrations, encompassing both minimal and maximal concentrations (Eleryan *et al.* 2022). The linear equation corresponding to this model is expressed in Equation 8.

$$\ln\frac{q_e}{q_m - q_e} = n\ln K_L + n\ln C_e \tag{8}$$

In this context, the variables are defined as follows:

- K_L and n are called the Toth isotherm constants in mg/g.
- q_e represents the measurement of adsorbed components at equilibrium in mg/L.

2.5. Adsorption kinetic studies

2.5.1. Pseudo first order

This kinetic or the Lagergren kinetic model determines the adsorption capacity within solid-liquid systems. It is based on the assumption that the desorption rate of azo dyes is directly proportional to the driving force (Khalid *et al.* 2019). Assessing the azo dye adsorption onto the biochar involved examining the change from the starting (q_e) to the balanced (q) concentrations of azo dye solutions. Equation 9 represents the Lagergren kinetic model for this process.

$$\frac{dq_e}{dq_t} = k(q_e - q_t) \tag{9}$$

After equilibrium attainment, the total amount of azo dye adsorbed by the rice husk biochar at a particular time (t) was determined by computing q_e and q_t. Equation 9 can be reformulated into Equation 10 by considering the boundary layer conditions.

$$\log(q_e - q) = \log q_e - \frac{k}{2.303}t \tag{10}$$

2.5.2. Pseudo second order

The second-order kinetic model was employed under the presumption that the adsorption rate is directly linked to unoccupied sites within the biochar adsorbent (Karimi *et al.* 2021). The equation representing the Pseudo-second-order kinetic model can be articulated as Equation 11.

$$\frac{d_q}{d_t} = k(q_e - q)^2 \tag{11}$$

Through the application of conditions set at the beginning (t = 0), extending beyond that point (t > 0), and going from q = 0 to q > 0, Equation 11 can be restructured into Equation 12.

$$\frac{t}{q} = \frac{1}{h} + \frac{1}{q_e}t \tag{12}$$

In this context, with h denoting the initial adsorption rate calculated as kq_e^2 and k representing the rate constant, creating a linear relationship by plotting t/qt against time

at different adsorption levels enables us to ascertain q_e, k, and h.

2.5.3. Boyd's kinetic study

Boyd's kinetic study is often referred to in evaluating water and wastewater treatment processes, mainly related to disinfection and chemical reactions. Boyd's kinetic study assesses the reaction rate of specific chemical processes in water treatment (Fideles *et al.* 2019). The Boyd method is typically used to determine the reaction order and rate constant of a chemical reaction occurring in a water treatment system. After getting the B values from the Boyd kinetic plots, the value of Di, which reflects the effective diffusion coefficient, may be determined using Equation 13.

$$Bt = -0.4977 - \ln(1-F) \tag{13}$$

3. Results and discussion

3.1. BET surface area analysis

The BET isotherm plot, shown in Figure 1, demonstrates a linear relationship between the adsorbed volume of N_2 and the relative pressure. This isotherm curve indicates that the adsorption process falls under the type-I category, suggesting the existence of fine or middle-sized apertures in the prepared biochar-activated adsorbent (Dulla *et al.* 2020). The Activated Rice Husk Biochar adsorbent boasts an impressive surface area of 96.585 m²/g, surpassing commercial activated carbons. Additionally, it exhibits a pore volume of 0.9740 cm³/g and a pore radius of 11.821 Å. For further comparison between biochar and activated Rice Husk Biochar adsorbent, please refer to Table 1.
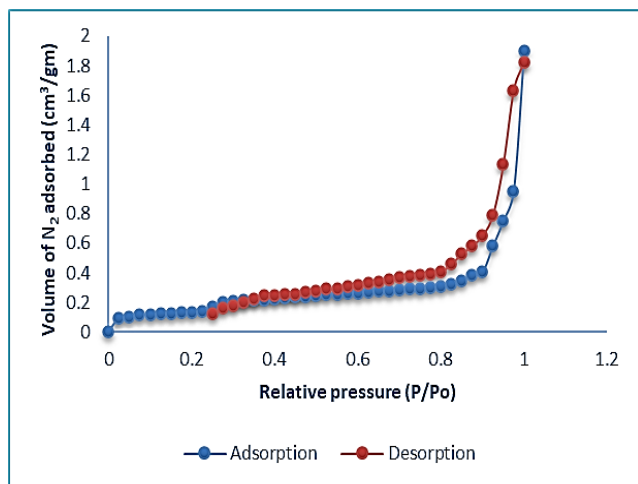

Figure 1. BET adsorption isotherm study of Activated Rice Husk Biochar powder

3.2. SEM analysis

The scanning electron microscopic analysis of raw Rice Husk Biochar powder, biochar, and activated biochar Rice Husk Biochar charcoal powder after absorbing the azo dyes Acid Brown and Methylene Blue is depicted in Figures 2a, 2b, and 2c, respectively. The presence of active sites is minimal in the SEM image of the raw adsorbent powder (Figure 2a). The active sites play a crucial role in adsorbing pollutants onto the exterior of the adsorbent

material. Figure 2b displays the SEM image of biochar powder before the activation process, while Figure 2c illustrates the SEM image of the activated biochar adsorbent material. These figures reveal that the activated biochar Rice Husk Biochar adsorbent material exhibits a significantly higher availability of active sites and surface area. In Figure 2c, one can observe the presence of uneven pores on the surface of the biochar-activated adsorbent. These pores are a result of the chemical activation process using hydrogen peroxide. They play a crucial role in attracting and receiving the separation of toxins from the liquid environment, enhancing the adsorption capacity of the material (Pham *et al.* 2021). Figure 2d displays the SEM images of the biochar-activated charcoal adsorbent after adsorbing azo dyes, indicating the changes in the surface structure due to the adsorption process. The biochar-activated Rice Husk Biochar adsorbent material exhibits an impressive capacity for adsorbing pollutants from aqueous solutions. As shown in Figure 2d, the surface of the biochar-activated adsorbent becomes wholly covered with pollutants, creating a cloud-like appearance on the top side. This suggests that the adsorbent surface has reached full occupancy, leaving no vacant sites available, indicating the successful completion of the adsorption process. Additionally, the synthetic dyes engage with the charged sites through interaction and undergo protonation without causing damage to the existing functional groups in the adsorbent material (Halim *et al.* 2019). The extent of adsorption of the specific dyes with azo compounds and the adsorbent material's reactivity was assessed through the following EDX analysis.

Table 1. Pore properties of unprocessed and activated rice husk biochar adsorbents

S. No.	Parameter	Units	Biochar Adsorbent
1.	BET surface area	m²/g	96.585
2.	Pore volume	cm³/g	0.9740
3.	Micropore volume	cm³/g	0.236
4.	Mesopore volume	cm³/g	0.112
5.	Micropore area	m²/g	438
6.	Average pore radius	Å	11.821

3.3. EDX analysis

Individual EDX analyses were conducted to validate the presence of the specific dyes with azo compounds in laboratory-synthesized solutions, assessing various conditions separately. Figure 3a displays the EDX image of the raw Rice Husk Biochar adsorbent, indicating the presence of organic and inorganic elements. Figure 3b reveals the prepared adsorbent material after activation with hydrogen peroxide following the biochar preparation (Kumar *et al.* 2013). Figure 3a confirms the presence of elements like carbon, oxygen, and calcium, while Figure 3b indicates the presence of other pollutants such as

chromium and aluminium. The synthetic solutions containing azo dyes were introduced to the activated biochar adsorbent, and the capacity to adsorb azo dye was evaluated, determining the quantity absorbed. The figure exhibits the EDX representation of the activated biochar adsorbent following the absorption of azo decontamination of the aqueous media. This analysis reveals the presence of additional organic and inorganic materials like magnesium, silicon, and iron.
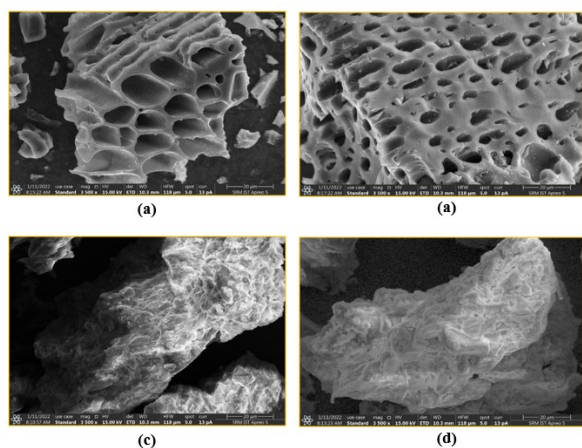

Figure 2. SEM images of (a) Rice husk adsorbent, (b) Biochar rice husk adsorbent, (c) Biochar adsorbent with chemical activation & (d) Activated biochar rice husk adsorbent with azo dyes adsorption respectively
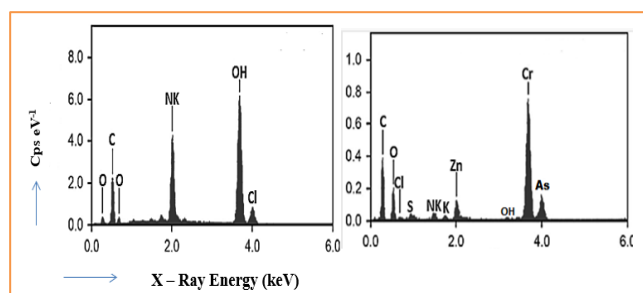

Figure 3. Energy Dispersive analysis of rice husk biochar adsorbent before and after the uptake of azo dyes

3.4. FTIR analysis

The FTIR functional groups were identified for the rice husk adsorbent, biochar, and acid-activated adsorbent, as shown in Figure 4 (a) and (b), respectively. The existence of a spectrum of functional clusters was analyzed based on the bandwidth in energy regions to understand the adsorption process better. The FTIR image shows a high-energy region with bandwidths at 3420 cm^{-1} and 2860 cm^{-1}, confirming the existence of -OH and -CH$_2$ functional groups. In the range from 1800 – 1000 cm^{-1}, various functional groups were identified, including water at 1620 cm^{-1}, aromatic vibrations between 1600 – 1400 cm^{-1}, -CH$_2$ bending vibrations between 1400 – 1380 cm^{-1}, and C-O vibrations at 1080 cm^{-1}. The -C-H bending caused by aromatic vibrations was detected at a bandwidth of 1000 cm^{-1}. Vibrations from the aromatic ring resulted in -OH stretching in lower-frequency regions, while the -CH$_2$ stretching vibrations ceased at the bandwidth of 2860 cm^{-1}. Therefore, the FTIR studies have confirmed the existence of Many organic and inorganic functional

components in the activated biochar Rice Husk Biochar adsorbent material (Djelloul *et al.* 2014). Additionally, it validates the adsorbent's capacity to eliminate impurities from the liquid environment via adsorption.
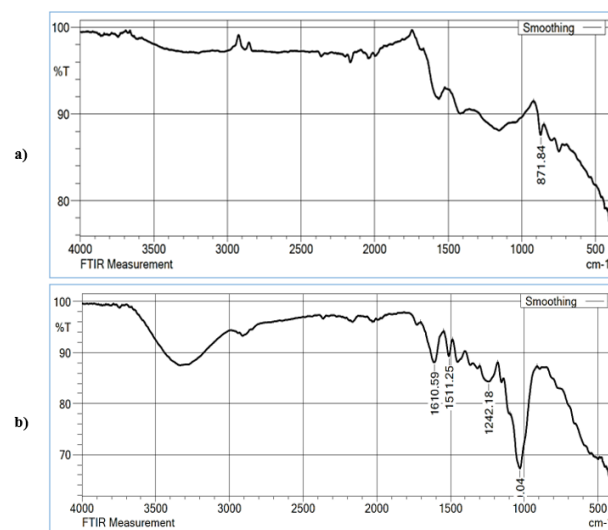

Figure 4. FTIR peaks of (a) Rice husk biochar & (b) azo dyes adsorbed rice husk biochar respectively

3.5. XRD analysis

Figure 5 (a) and (b) depict the XRD peaks of the raw and activated biochar Rice Husk Biochar adsorbent, respectively. When comparing the XRD figures, it is evident that the raw adsorbent exhibits a shallow crystalline structure and intensity in contrast to the activated biochar adsorbent. The activated biochar adsorbent strongly agreed with the XRD peaks at 150, 220, 260, 290, 355, and 420 at 2θ, corresponding to the 80, 110, 50, 30, 25, and 20 planes. This crystalline structure significantly enables the adsorbent to effectively retain pollutants captured from the water solution (Boubaker *et al.* 2021). The activated biochar adsorbent possesses a significantly higher degree of crystallinity than the unprocessed adsorbent. The activated biochar adsorbent exhibits much higher intensity, resulting in pronounced diffraction patterns and more prominent peaks.
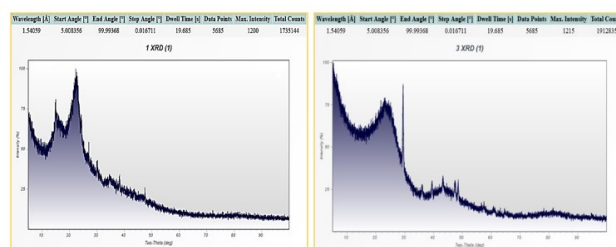

Figure 5. XRD diffractions of (a) Raw & (b) Activated biochar adsorbent

3.6. Impact of pH in azo dye removal

During the batch-wise adsorption assessment, the implication of azo dye uptake was evaluated by varying the pH values from 2.0 to 12.0, keeping the azo dye concentration, biochar adsorbent dose, contact time, and temperature constant. Figure 6 illustrates that a decrease

in the pH of the azo dye solution resulted in an elevation adsorptive removal of azo dyes using activated biochar. This phenomenon can be attributed to the increased interaction between azo dyes and the negatively charged adsorbent surface at lower pH levels. The adsorbent's surface develops a high positive charge at very high solution pH levels, which may contribute to the rapid removal of azo dyes (Manjuladevi *et al.* 2018). The biochar adsorbent adsorbed the highest quantity of the desired azo dyes at a pH of 10.0. At elevated pH levels, there is a phenomenon of hydroxide precipitation, leading to a decrease in the adsorption of azo dyes by the biochar adsorbent. This research discovered that the activated biochar adsorbent effectively eliminated 88.02% of Acid Brown and 94.42% of Methylene Blue azo dyes from the synthetic solution when maintained at the optimal pH level 10.0.
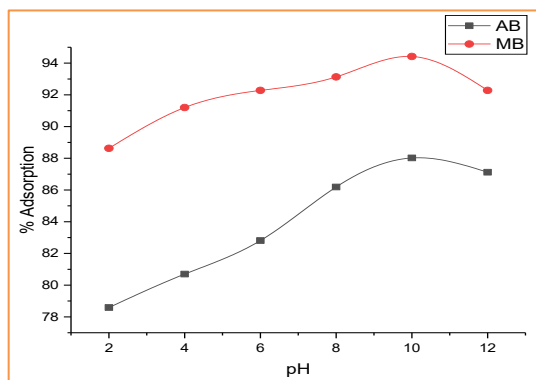

Figure 6. Adsorption of Acid Brown &Methylene Blue dyes by varying the pH using activated biochar Rice Husk Biochar

3.7. Impact of biochar dose in dye removal

The study explored the influence of changing the activated biochar dosage within the range of 1.5 g/L to 3.5 g/L at intervals of 0.5 g/L. At the same time, all other parameters, including pH, contact time, azo dye concentration, and temperature, remained unchanged. Figure 7 demonstrates the effect of azo dye adsorption as the activated biochar concentration varies. It's noticeable that there is a gradual decline in dye adsorption as the adsorbent quantity is decreased. At lower dosage levels, there is a notable scarcity of active sites, leading to a diminished uptake of the extraction of azo dye from water, as reported by Langeroodi *et al.* 2018. At the ideal biochar concentration of 3 g/L, the adsorbent accomplished an 80.48% reduction in Acid Brown and a 70.28% reduction in Methylene Blue azo dyes. Past the three g/L threshold, the absorption of azo dye levelled off because of a decline in the concentration gradient. The presence of an unoccupied surface area during the absorption of azo dye by the biochar contributes to the formation of the concentration gradient.

3.8. Impact of contact time in dye removal

The contact time during the adsorption process can influence the interaction between the adsorbent and pollutants. When the interaction time is prolonged, the amount of pollutant uptake by the adsorbent tends to increase. The concentrations of each azo dye were adjusted from 20 mg/L to 100 mg/L, and the timeframe of

interaction between the biochar adsorbent and the dyes was tuned from 10 minutes to 1 hour. Figure 8 showcases the influence of the extent of azo dye assimilation from the aqueous solutions. During the initial stages, the activated biochar adsorbent showed notable azo dye adsorption, mainly attributable to the heightened abundance of active sites. After 60 minutes of contact time, there was a reduction in the elimination of azo dyes from the aqueous solutions. They were eventually reaching a saturation point. This decline can be attributed to the limited availability of vacant sites and the repulsive forces acting on the surfaces of adsorbent molecules (Biswas *et al.* 2015). Furthermore, during the later stages of contact time, the azo dye uptake decreases as the dye molecules require more energy to penetrate the pores of the biochar adsorbent.
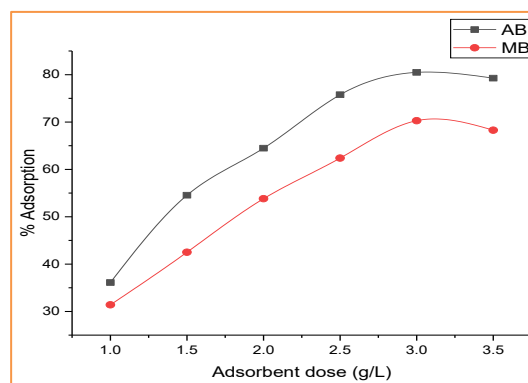

Figure 7. Adsorption of Acid Brown and methylene Blue dyes by varying the activated biochar dose

3.9. Impact of dye concentration in adsorption

With a pH of 10.0, a contact time of 60 minutes, and a biochar adsorbent dose of 3 g/L, the azo dye concentrations varied from 20 mg/L to 100 mg/L to assess their impact on biochar uptake. As shown in Figure 9, when the azo dye concentration was low in the initial stages, the quantity of dye absorption by the biochar adsorbent was exceptionally substantial. This can be credited to the profusion of active locations on the surface of the adsorbent. A sharp decrease in dye uptake was observed as the concentration of azo dye solutions increased. This decline is linked to the saturation of mesopores with adsorbed azo dyes (Fakhar *et al.* 2021). The biochar activated from Rice Husk Biochar adsorbed 88.45% of Acid Brown and 90.12% of Methylene Blue category azo dyes at low concentrations. This rapid uptake of azo dyes by the adsorbent at low concentrations suggests that the biochar adsorbent did not reach its saturation point.
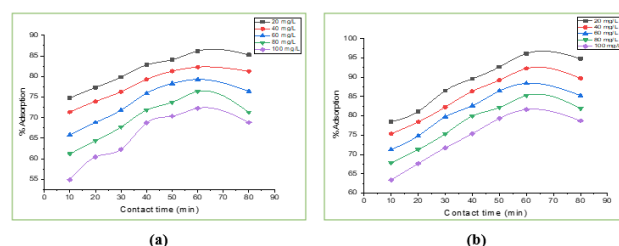

Figure 8. Adsorption of Acid Brown & Methylene Blue with contact time variations
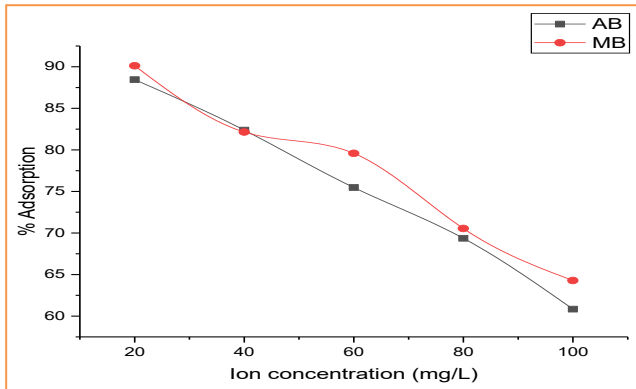
Figure 9. Adsorption of Acid Brown, Reactive Red and methylene Blue dyes by varying the concentration of azo dyes

3.10. Isotherm studies

3.10.1. Langmuir isotherm

Figure 10 displays the straight-line graphs for the Langmuir adsorption isotherm model (C_e/q_e vs. C_e), and the constants of this model (k and q_{max}) were derived from the slope and intercept of these linear plots. The regression coefficient values acquired from the Langmuir kinetic plots at a temperature of 30°C are listed in Table 2. Figure 10 illustrates the linear Langmuir isotherm plots (C_e/q_e vs. C_e), and the model's constants (k and q_{max}) were computed using the incline and intercept of these straight-line graphs. The coefficient of regression values obtained from the Langmuir kinetic plots at a temperature of 30°C are presented in Table 2.
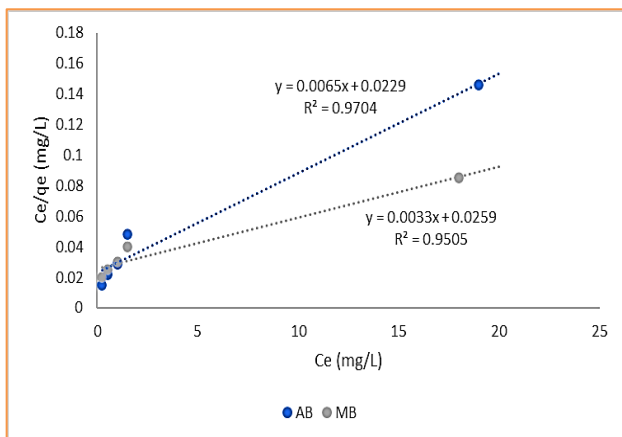

Figure 10. Langmuir plot for AB & MB adsorption using rice husk biochar

3.10.2. Freundlich isotherm

The linear plots in Figure 11 depict the Freundlich isotherm model (ln qe vs. ln Ce), and the constants of the model (K_f and n) have been computed by examining the slopes and intercepts of these plots. The coefficient of regression values obtained from the Freundlich kinetic plots at a temperature of 30°C can be found in Table 2. The values of n, 3.580 for Acid Brown and 2.658 for Methylene Blue, all fall from 1 to 10. This suggests that azo dye uptake follows physical adsorption rather than chemical adsorption (Su *et al.* 2021). The high correlation between the experimental data and the Langmuir and Freundlich plots, as evidenced by the high regression

values (R^2), suggests that these models are applicable and that the adsorption process follows physical adsorption.
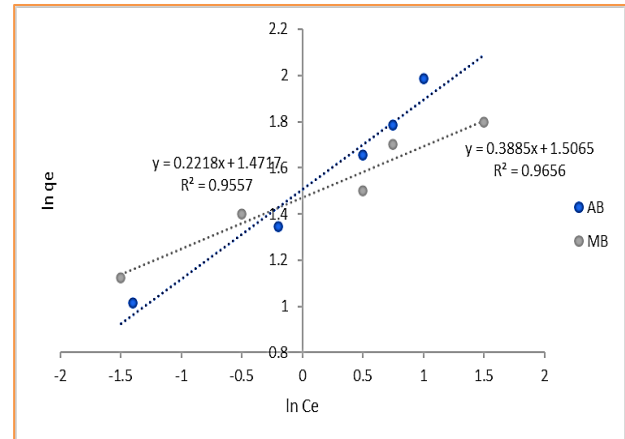

Figure 11. Freundlich plot for AB & MB adsorption using rice husk biochar

3.10.3. R-P isotherm

Figure 12 showcases the linear plots for the R-P isotherm model, and the constants (K_R and a_R) have been derived from the slopes and intercepts of these linear plots, as detailed in Table 2. This model offers significantly higher accuracy with its three unknown parameters than other isotherm models (Obulapuram *et al.* 2021). The choice between Langmuir and Freundlich fitting for the adsorption process can be determined by examining the values of b_R, which fall within the range of 0 to 1. Table 2 reveals that the b_R values exceed 1, suggesting that azo dye adsorption by the biochar adsorbent adheres to a heterogeneous monolayer adsorption pattern.
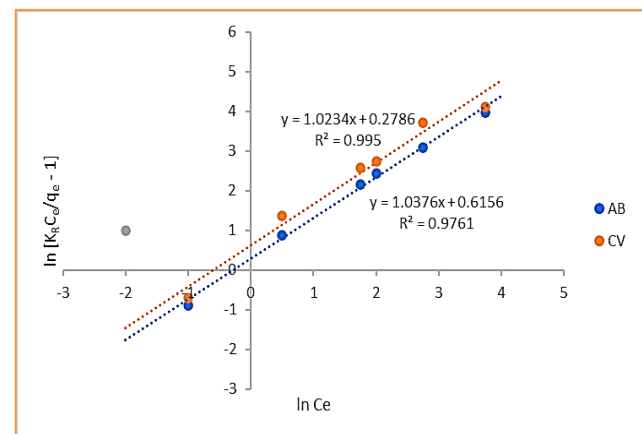
Figure 12. R-P isotherm plot for AB & MB adsorption using rice husk biochar

3.10.4. Sips isotherm

Figure 13 displays the linear plots of the Sips isotherm model, and the model's constants were determined and are listed in Table 2. Based on the variability index (n) obtained from this model's linear plots, the adsorption process's attribute was determined to be either heterogeneous or homogeneous (Hashemian *et al.* 2013). The high regression values (R^2) obtained from the linear plots, all exceeding 0.95, confirm the suitability of the Sips isotherm model for the data. The 'n' value, falling from 0 to 1, suggests a fitting between the Langmuir and

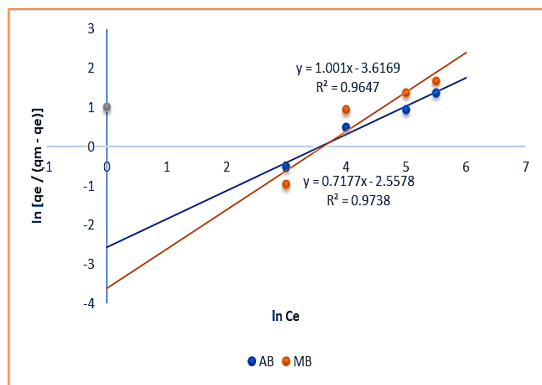Freundlich isotherms. When n = 1, it indicates conformity with the Langmuir isotherm fit.

Figure 13. Sips plot for AB & MB adsorption using rice husk biochar

3.10.5. Toth isotherm

The Toth isotherm study was utilized to distinguish the non-identical characteristics of the solid surface, and the corresponding constant values were determined. Figure 14 illustrates the linear plots corresponding to the Toth isotherm model, while Table 2 provides the associated constants for this model, including Q_{max}, b_T, and n_T. Three parameters were extracted from the linear plots, and this model is frequently referred to as a three-parameter model, offering a high level of accuracy in fitting the isotherm. The Toth isotherm model was employed to analyze the interaction between the biochar adsorbent surfaces and azo dye pollutants. However, the obtained regression values (R^2) from the linear plots were lower than 0.95, indicating that this model did not adequately fit the adsorption process. When the Langmuir isotherm data is in excellent agreement with the equilibrium data, and linear plots are obtained with the Toth isotherm were utilized to establish a connection within the adsorption process of azo dye, the equilibrium by the biochar adsorbent (Kromah *et al.* 2021). However, the Langmuir data fitting was successful in this adsorption process, making it unnecessary to verify the favourable correlation of the adsorption process with the Toth isotherm examination.
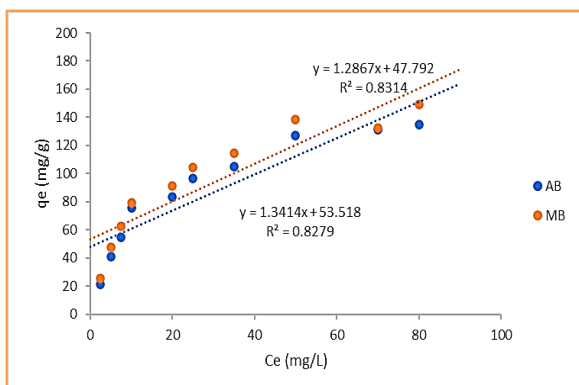

Figure 14. Toth isotherm plot for AB & MB adsorption using rice husk biochar

3.10.6. Fritz-schlunder isotherm

The study involved an analysis of adsorption variations concerning temperature and pressure, utilizing the four-parameter isotherm model known as the Fritz-Schlunder model. Figure 15 displays the linear plots from this isotherm analysis, while Table 2 presents the obtained constants. The high regression values (R^2), exceeding 0.95, signify the suitability of this isotherm model. Furthermore, the constants acquired from the linear plots align well with the adsorption process, demonstrating agreement. The mentioned isotherm studies were employed to assess whether the adsorption process exhibits a favourable nature, as outlined by Yogeshwaran et al. in 2021. The results of these studies indicate that the Langmuir, Freundlich, R-P, Sips, and Fritz-Schlunder models are well-suited for describing the adsorption of azo dye, suggesting a monolayer adsorption mechanism within a heterogeneous context.
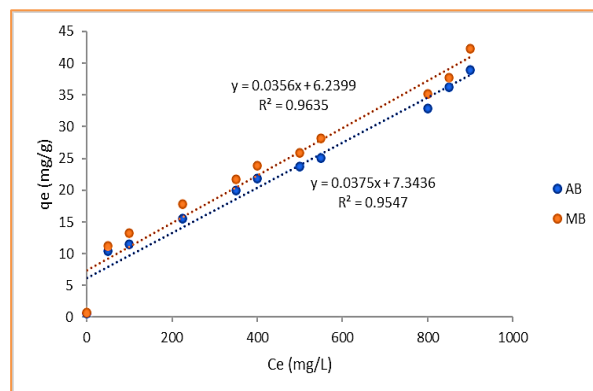

Figure 15. Fritz-Schlunder isotherm plots for AB & MB adsorption using rice husk biochar

3.11. Kinetic studies

3.11.1. Pseudo – first order kinetic study

The adsorption kinetics for Acid Brown and Methylene Blue azo dyes can be characterized using the Pseudo-first-order kinetic model, which involves plotting [(qe – q) vs. t]. Figure 16 (a) & (b) illustrates the kinetic plots for Pseudo-first-order studies of azo dye uptake using activated Rice Husk Biochar as the adsorbent. This kinetic model's constant (k) was determined by varying the azo dye concentrations from 25 mg/L to 150 mg/L. The regression values (R^2) were computed based on the kinetic plots. Table 3 provides an overview of the obtained constants (k) and regression values (R^2), and it was observed that these values align well with the adsorption process, exhibiting high levels of agreement, all exceeding 0.95. This suggests that the kinetic model is applicable and indicates the attainment of the adsorption process and its saturation level.

3.11.2. Pseudo – second order kinetic study

This kinetic model also employed the same azo dye concentrations (ranging from 25 – 150 mg/L) utilized in the Pseudo-first-order studies. This consistency in the concentration range allowed for the evaluation of using the activated biochar adsorbent for the adsorption process of azo dye. The kinetic plots (t/q vs. t) for this model are presented in Figure 16 (c) & (d), and the corresponding constants have been acquired and are documented in Table 3. Similar to the first-order studies, the constants for the adsorption process displayed a

robust correlation with the pseudo-second-order kinetic model. Furthermore, the calculated R^2 values exceeding 0.95 confirm the applicability of this kinetic study, as reported by Batagarawa *et al.* 2019. Considering the applicability of both Pseudo-first-order and Pseudo-second-order kinetics, it can be inferred that the adsorption process has reached a saturation condition regarding removing azo dye from synthetic solutions.

Table 2. Constants for isotherms in the adsorption of azo dye using activated rice husk biochar

S. No.	Model	Parameters	Acid Brown	Methylene Blue
1.	Langmuir	q_{max}	10.353	11.832
		K_L	0.434	0.184
		R^2	0.9704	0.9505
2.	Freundlich	K_f	2.895	1.832
		n	3.143	2.246
		R^2	0.9557	0.9656
3.	Redlich-Peterson (R-P)	K_{RP}	13.2367	5.6351
		α_{RP}	0.5468	0.0989
		β_{RP}	1.4821	1.4139
		R^2	0.995	0.9761
4.	Sips	K_S	16.8235	4.0931
		β_S	1.4923	1.9731
		a_S	0.6012	0.1602
		R^2	0.9647	0.9738
5.	Toth	Q_{max}	31.2731	25.8234
		b_T	0.4533	0.1932
		n_T	0.9732	0.5083
		R^2	0.8314	0.8279
6.	Fritz-Schlunder	Q_{MFS}	0.4389	0.0940
		K_{FS}	57.372	73.643
		N_{FS}	1.1273	1.3291
		R^2	0.9635	0.9547

Table 3. Kinetic Constants for azo dyes adsorption using rice husk biochar

S. No.	Name of the metal ion	Conc.(mg/L)	Pseudo First Order			Pseudo Second order			Boyd		
			K / min	Exp. q_e (mg g^{-1})	$K \times 10^{-3}$ (g mg^{-1})	R^2	Cal. q_e (mg/g)	h (mg g^{-1} min^{-1})	R^2	B	D_i (x 10^{-3} m^2/s)	R^2
1.	AB	25	0.034	2.64	0.95	16.69	2.15	0.10	0.96	0.034	5.472	0.915
2.		50	0.043	7.02	0.93	5.73	5.19	0.18	0.98	0.044	7.340	0.973
3.		75	0.041	10.00	0.93	3.34	8.30	0.22	0.98	0.043	7.621	0.963
4.		100	0.039	11.36	0.94	5.07	10.75	0.26	0.98	0.039	6.856	0.914
5.		125	0.048	17.47	0.92	2.00	12.91	0.29	0.97	0.049	8.725	0.982
6.		150	0.045	19.43	0.93	3.12	13.82	0.30	0.96	0.045	7.452	0.952
7.	MB	25	0.046	3.68	0.91	12.62	2.70	0.10	0.97	0.046	7.678	0.943
8.		50	0.041	6.54	0.93	5.32	5.47	0.12	0.98	0.041	6.294	0.983
9.		75	0.043	9.95	0.92	3.56	8.60	0.23	0.98	0.045	7.959	0.924
10.		100	0.046	12.38	0.94	2.77	10.10	0.28	0.97	0.046	7.678	0.983
11.		125	0.052	20.55	0.92	2.30	11.56	0.31	0.98	0.053	8.590	0.941
12.		150	0.050	25.48	0.94	2.65	12.73	0.33	0.96	0.055	8.972	0.922

3.11.3. Boyd kinetic model

The graphs in Figure 16 (e) and (f) demonstrate the connection between Bt and t, which is a standard technique to analyze the removal of pollutants (AB and MB) using rice husk biochar at varied concentrations. These plots are circular and, significantly, do not cross the origin point. This data implies that the removal of contaminants in the adsorption process is not primarily regulated by intra-particle diffusion, as suggested by Saruchia *et al.* 2019. When examining Bt versus t plots, it's customary to assess the role of intra-particle diffusion in removing metal ions or other pollutants. A linear plot of Bt versus t that passes through the origin typically indicates that intra-particle diffusion is the controlling step in the adsorption process. In this case, since the plots are circular and do not intersect the origin, it suggests that intra-particle diffusion is not the primary rate-determining step. Other mechanisms or factors are likely in the adsorption of the pollutants AB and MB using rice husk biochar.
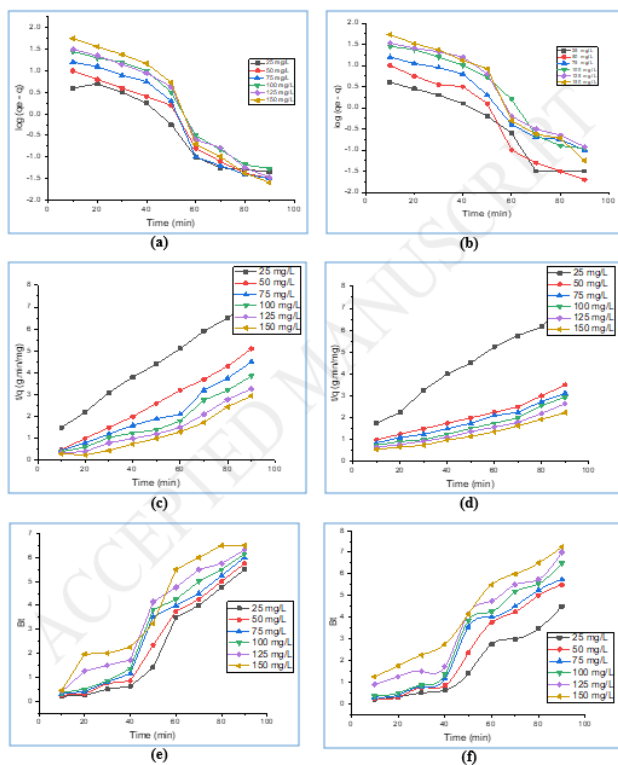

Figure 16. (a) & (b) Pseudo first order, (c) & (d) Pseudo second order and (e) & (f) Boyd kinetic plots for Acid Brown and Methylene Blue azo dye uptake using activated Rice Husk Biochar

3.12. Thermodynamic and temperature studies

The concentration of the azo dye solution was adjusted over a temperature range of 15°C to 45°C, and the effect of these temperature changes on the evaluation of azo dye adsorption by the biochar adsorbent was conducted across various operational settings, including Figure 17, depicts the influence of temperature fluctuations on the elimination of azo dye from synthetic solutions by using activated biochar as an adsorbent. A notable increase in azo dye uptake is observed as the temperature reaches 20°C. However, there is no further change in azo dye

adsorption beyond this point, indicating a saturation or plateau in adsorption efficiency. The decrease in dye adsorption beyond 20°C can be attributed to the exothermic nature of the process and a reduction in the available surface area of the biochar adsorbent, as discussed by Alqadami *et al.* 2017. Figure 18 displays the thermodynamic plots for the azo dye adsorption process using biochar-activated carbon as the adsorbent. The derived values for the slope and intercept, representing the changes in enthalpy (ΔH_o) and entropy (ΔS_o), respectively, have been calculated from these plots and are provided in Table 4. The negative ΔG_o values and positive ΔH_o values indicate the inherent spontaneity of the activated biochar adsorbent material and indicate that the adsorption process is endothermic, as discussed by Elmi *et al.* 2020. Additionally, positive ΔS_o values highlight the significance of the interaction between solid and liquid particles in the adsorption process and underscores its role in the process's uncertainty.
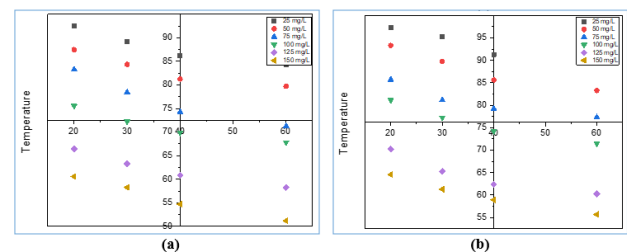

Figure 17. Impact of temperature in (a) Acid Brown & (b) Methylene Blue dye adsorption using activated biochar Rice Husk Biochar
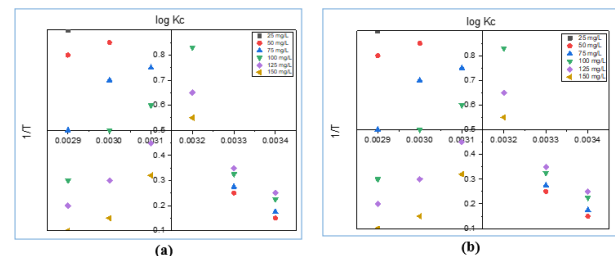

Figure 18. Thermodynamic plots for (a) Acid Brown & (b) Methylene Blue dye adsorption using activated biochar Rice Husk Biochar

3.13. Desorption studies

An essential step in adsorption investigations is the recovery of adsorbed azo dyes and used adsorbent. The dyes and biochar adsorbent material were recovered using concentrated hydrochloric acid, and the amount of azo dyes desorbed by the HCl solution is shown in Table 5, together with the normalcy of the HCl solution, which ranges from 0.1 to 0.4. By adding 0.3N of HCl acid, the maximum amount of azo dye recovery could be seen. However, when the concentration increased past 0.3N, a rapid decrease in recovery could be seen; when the concentration of HCl rose, the recovery rate of azo dyes reached a steady level. So, by adding 0.3N of HCl acid, the highest level of azo dye recovery was achievable, and the recovered azo dyes were put to use in more experimental research.

Table 4. The thermodynamic constants for the adsorption of azo dyes using powdered activated charcoal derived from Rice Husk Biochar

Initial concentration of AB Dye (mg/L)	Enthalpy (ΔH°) KJ mol^{-1}	Entropy (ΔS°) J mol^{-1}	Gibbs Energy (ΔG$_o$) kJ mol^{-1}			
			15°C	30°C	45°C	60°C
25	82.284	190.203	−16.390	−11.329	−10.590	−8.466
50	39.249	97.042	−11.812	−9.536	−8.389	−7.125
75	24.393	48.993	−9.485	−8.420	−7.413	−6.002
100	15.821	31.417	−6.030	−6.959	−5.955	−4.682
125	11.299	29.055	−4.112	−4.067	−3.698	−3.011
150	9.205	24.273	−2.902	−2.236	−2.070	−2.212
The initial concentration of MB dye (mg/L)						
25	75.707	170.506	−13.495	−11.663	−9.542	−8.345
50	42.557	85.237	−11.403	−10.485	−8.632	−7.432
75	25.208	38.994	−9.570	−8.699	−7.907	−6.982
100	17.033	20.340	−7.884	−6.128	−5.473	−4.438
125	12.473	15.219	−5.358	−4.691	−3.756	−3.034
150	8.782	9.506	−4.317	−3.260	−2.967	−2.348

Table 5. The removal of azo dyes from activated biochar Rice Husk Biochar through desorption

Initial concentration (25 mg/L)	Recovery of azo dyes (%)	Concentration of HCl			
		0.10 N	0.20 N	0.30 N	0.40 N
		% Desorption of azo dyes			
Acid Brown	88.04	67.12	70.24	73.54	69.58
Methylene Blue	94.41	71.51	75.64	80.25	78.53

4. Conclusion

Azo dyes were removed from aqueous solutions by employing biochar as an adsorbent in activated rice husk. These are the results from the batch mode of the research. Under a pH of 10.0, a biochar dose of 3 g/L, an azo dye concentration of 25 mg/L, and a 60-minute interval for exposure, the highest level of azo dye adsorption from synthetic solutions was achieved. Throughout the entire batch adsorption studies, the temperature of the solution was maintained at a constant 30°C. The adsorption process exhibited a robust correspondence with the Langmuir, Freundlich, R-P, Sips, and Fritz-Schlunder isotherm investigations. The Pseudo-first and Pseudo-second-order kinetic studies displayed strong regression models that matched the adsorption process well. The rice husk biochar adsorbent efficiently removes Acid Brown (88%), Reactive Red and Methylene Blue (94%) azo dyes. The highest azo dye recovery was attained by introducing 0.3 N hydrochloric acid to the exhausted adsorbent.

References

Abdel Halim A., El-Ezaby K. and El-Gammal M. (2019). Removal of Fe^{2+} and Pb^{2+} ions from wastewater using rice husk based adsorbents. *Journal of Egypt Academy of Societry and Environmental Development* **20**, 47–60. Doi: 10.21608/JADES.2019.67694

Alqadami A.A., Naushad M., Abdalla M.A., Ahamad T., ALOthman Z.A., Alshehri S.M. and Ghfar A.A. (2017). Efficient removal of toxic metal ions from wastewater using a recyclable nanocomposite: A study of adsorption parameters and interaction mechanism, *Journal of Cleaner Production*, **156**, 426–436. https://doi.org/10.1016/j.jclepro.2017.04.085

Batagarawa S.M. and Ajibola, A. K. (2019). Comparative evaluation for the adsorption of toxic heavy metals on to millet, corn and rice husks as adsorbents. *Journal of Analytical and Pharmaceutical Research*, **3**, 119–125. Doi: 10.15406/japlr.2019.08.00325

Biswas S. and Mishra U. (2015). Continious fixed bed column study and adsorption modeling: removal of lead ion from aqueous solution by charcoal originated from chemical carbonization of rubber wood sawdust. *Journal of chemistry* ID: 907379. Doi: https://doi.org/10.1155/2015/907379.

Boubaker H., Arfi R.B., Mougin K., Vaulot C., Hajjar S., Kunneman P. and Ghorbal A. (2021). New optimization approach for successive cationic and anionic dyes uptake using reed-based beads, *Journal of Cleaner Production*, **307**, 127218. https://doi.org/10.1016/j.jclepro.2021.127218

Bouras H.D., Benturki O., Bouras N., Attou M., Donnot A., Merlin A. and Holtz M.D. (2015). The use of an agricultural waste material from Ziziphus jujuba as a novel adsorbent for humic

acid removal from aqueous solutions. *Journal of Molecular Liquids*, **211**, 1039–1046. Doi: https://doi.org/10.1016/j.molliq.2015.08.028

Djelloul C. and Hamdaoui O. (2014). Dynamic adsorption of methylene blue by melon peel in fixed-bed columns, *Desalination and Water Treatment*, **56**, 2966–2975. https://doi.org/10.1080/19443994.2014.963158

Dulla J.B., Tamana M.R., Boddu S., Pulipati K. and Srirama K. (2020). Biosorption of copper (II) onto spent biomass of Gelidiella acerosa (brown marine algae): optimization and kinetic studies, *Applied Water Science*, **10** (56). https://doi.org/10.1007/s13201-019-1125-3

Eleryan A., Aigbe U.O., Ukhurebor K. E., Onyancha R.B., Eldeeb T.M., El-Nemr M.A. and El Nemr A.. (2022). Copper(II) ion removal by chemically and physically modified sawdust biochar. *Biomass Conversion and Biorefinery*. https://doi.org/10.1007/s13399-022-02918-y

Elmi F., Mohammadi Damghani F. and Shokrollahzadeh Taleshi M. (2020). Kinetic and Isotherm Studies of Adsorption of the Metribuzin Herbicide on an Fe_3O_4/CNT@PDA Hybrid Magnetic Nanocomposite in Wastewater, *Industrial and Engineering Chemistry Research*, **59** (20), 9604–9610. https://doi.org/10.1021/acs.iecr.9b07077

Fakhar N., Khan S.A., Siddiqi W.A. and Khan T.A. (2021). Ziziphus jujube waste-derived biomass as cost-effective adsorbent for the sequestration of Cd^{2+} from aqueous solution: Isotherm and kinetics studies. *Environmental Nanotechnology, Monitoring & Management*, **16**, 100570. Doi: https://doi.org/10.1016/j.enmm.2021.100570

Fideles R.A., Teodoro F.S., Xavier A. L.P., Adarme O.F.H., Gil L.F. and Gurgel L.V.A. (2019). Trimellitated sugarcane bagasse: A versatile adsorbent for removal of cationic dyes from aqueous solution. Part II: Batch and continuous adsorption in a bicomponent system, *Journal of Colloid and Interface Science*, **552** (15), 752–763. https://doi.org/10.1016/ j.jcis.2019.05.089

Hashemian S., Salari K., Salehifar H. and Yazdi A.Z. (2013). Removal of Azo Dyes (Violet B and Violet 5R) from Aqueous Solution Using New Activated Carbon Developed from Orange Peel, *Journal of Chemistry*, 283274. https://doi.org/10.1155/2013/283274

Karimi-Maleh H., Ayati A., Davoodi R., Tanhaei B., Karimi F., Malekmohammadi S and Sillanpaa M. (2021). Recent advances in using of chitosan-based adsorbents for removal of pharmaceutical contaminants: A review, *Journal of Cleaner Production*, **291**, 125880. https://doi.org/10.1016/ j.jclepro.2021.125880

Khalid M.W. and Salman S.D. (2019). Adsorption of Heavy Metals from Aqueous Solution onto Sawdust Activated Carbon. *Al-Khwarizmi Engineering Journal*, **15** (3), 60–69. https://doi.org/10.22153/kej.2019.04.001

Khan T.A., Nouman M., Dua D., Khan S.A. and Alharthi S.S. (2022). Adsorptive scavenging of cationic dyes from aquatic phase by H_3PO_4 activated Indian jujube (Ziziphus mauritiana) seeds based activated carbon: Isotherm, kinetics, and thermodynamic study, Journal of Saudi Chemical Society, **26** (2), 101417. https://doi.org/10.1016/j.jscs.2021.101417

Kromah V. and Zhang G. (2021). Aqueous Adsorption of Heavy Metals on Metal Sulfide Nanomaterials: *Synthesis and Application, Water*, **13** (13), 1843. https://doi.org/10.3390/ w13131843

Kumar M. and Tamilarasan R. (2013). Kinetics and Equilibrium Studies on the Removal of Victoria Blue Using Prosopis juliflora-Modified Carbon/Zn/Alginate Polymer Composite Beads, *Journal of Chemical & Engineering Data*, **58**, 517–527. dx.doi.org/10.1021/je3012309

Kumar M., Singh A.K. and Sikandar M. (2019). Biosorption of Hg (II) from aqueous solution using algal biomass: *Kinetics and isotherm studies, Heliyon*, **6** (1), e03321. https://doi.org/10.1016/j.heliyon.2020.e03321

Labied R., Benturki O., Hamitouche A.Y.E. and Donnot A. (2018). Adsorption of hexavalent chromium by activated carbon obtained from a waste lignocellulosic material (Ziziphus jujuba cores): Kinetic, equilibrium, and thermodynamic study. *Adsorption Science and Technology*, **36** (3–4), 1066–1099. Doi:10.1177/0263617417750739

Manjuladevi M., Anitha R. and Manonmani S. (2018). Kinetic study on adsorption of Cr (VI), Ni (II), Cd (II) and Pb (II) ions from aqueous solutions using activated carbon prepared from cucumis melo peel. *Applied water science*, **8**, 36. Doi: https://doi.org/10.1007/s13201-018-0674-1.

Mwandira W., Nakashima K., Kawasaki S., Arabelo A., Banda K., Nyambe I., Chirwa M., Ito M., Sato T., Igarashi T., Nakata H., Nakayama S. and Ishizuka M. (2020). Biosorption of Pb (II) and Zn (II) from aqueous solution by Oceanobacillus profundus isolated from an abandoned mine, *Scientific Reports*, **10**, 21189. https://doi.org/10.1038/s41598-020-78187-4

Nathan R.J., Martin C.E., Barr D. and Rosengren R.J. (2021). Simultaneous removal of heavy metals from drinking water by banana, orange and potato peel beads: a study of biosorption kinetics, *Applied Water Science*, **11** (116). https://doi.org/10.1007/s13201-021-01457-7

Obulapuram K.P., Arfin T., Mohammad F., Khiste S.K., Chavali M., Albalawi A.N. and Al-Lohedan H.A. (2021). Adsorption, Equilibrium Isotherm, and Thermodynamic Studies towards the Removal of Reactive Orange 16 Dye Using Cu(I)-Polyaninile Composite, *Polymers*, **13** (20), 3490. https://doi.org/10.3390/polym13203490

Panda L., Jena S.K., Rath S.S. and Misra P.K. (2020). Heavy metal removal from water by adsorption using a low-cost geopolymer, *Environmental Science and Pollution Research*, **27**, 24284–24298. https://doi.org/10.1007/s11356-020-08482-0

Pham B.N., Kang J.K., Lee C.G. and Park S.J. (2021). Removal of Heavy Metals (Cd^{2+}, Cu^{2+}, Ni^{2+}, Pb^{2+}) from Aqueous Solution Using Hizikia fusiformis as an Algae-Based Bioadsorbent, *Applied Sciences*, **11** (18), 8604. https://doi.org/10.3390/ app11188604

Priya A.K., Yogeshwaran V., Rajendran S., Hoang T.K., Soto-Moscoso M., Ghfar A.A. and Bathula C. (2022). Investigation of mechanism of heavy metals (Cr6+, Pb2+ & Zn2+) adsorption from aqueous medium using rice husk ash: Kinetic and thermodynamic approach, *Cshemosphere*, **286**, 131796, https://doi.org/10.1016/j.chemosphere.2021.131796

Regti A., Laamari M.R., Stiriba S.E. and El Haddad M. (2017). The potential use of activated carbon prepared from Ziziphus species for removing dyes from waste waters. *Applied Water Science*, **7**, 4099–4108. Doi: https://doi.org/10.1007/s13201-017-0567-8

Samadani Langeroodi N., Farhadravesh Z. and Dehno Khalaji A. (2018). Optimization of adsorption parameters for Fe (III) ions removal from aqueous solutions by transition metal oxide nanocomposite. *Green chemistry letters and reviews*, **11** (4), 404–413. Doi: https://doi.org/10.1080/17518253.2018.1526329

Saruchia and Vaneet Kumar. (2019). Adsorption kinetics and isotherms for the removal of rhodamine B dye and Pb^{+2} ions from aqueous solutions by a hybrid ion-exchanger, *Arabian Journal of Chemistry*, **12** (3), 316–329. https://doi.org/10.1016/j.arabjc.2016.11.009

Su L., Zhang H., Oh K., Liu N., Luo Y., Cheng H. and He X. (2021). Activated biochar derived from spent Auricularia auricula substrate for the efficient adsorption of cationic azo dyes from single and binary adsorptive systems, *Water Science & Technology*, **84** (1), 101–121. https://doi.org/10.2166/wst.2021.222

Tejada-Tovar C., Villabona-Ortíz Á. and Gonzalez-Delgado Á.D. (2021). Adsorption of Azo-Anionic Dyes in a Solution Using Modified Coconut (Cocos nucifera) Mesocarp: *Kinetic and Equilibrium Study, Water*, **13**, 1382. https://doi.org/10.3390/w13101382

Venkatraman Y. and Priya A.K. (2021). Removal of heavy metal ion concentrations from the wastewater using tobacco leaves coated with iron oxide nanoparticles, *International Journal of Environmental Science and Technology*, **19**, 2721–2736. https://doi.org/10.1007/s13762-021-03202-8

Xia L., Zhou S., Zhang C., Fu Z., Wang A., Zhang Q. and Xu W. (2020). Environment-friendly Juncus effusus-based adsorbent with a three-dimensional network structure for highly efficient removal of dyes from wastewater, *Journal of Cleaner Production*, **259**, 120812. https://doi.org/10.1016/j.jclepro.2020.120812

Yogeshwaran V. and Priya A.K (2021). Experimental studies on the removal of heavy metal ion concentration using sugarcane bagasse in batch adsorption process. *Desalination and Water Treatment*, **224**, 256–272. Doi: 10.5004/dwt.2021.27160